

RESEARCH ARTICLE

Three-dimensional shape and velocity changes affect responses of a locust visual interneuron to approaching objects

Tarquin P. Stott, Erik G. N. Olson, Rachel H. Parkinson and John R. Gray*

ABSTRACT

Adaptive collision avoidance behaviours require accurate detection of complex spatiotemporal properties of an object approaching in an animal's natural, three-dimensional environment. Within the locust, the lobula giant movement detector and its postsynaptic partner, the descending contralateral movement detector (DCMD), respond robustly to images that emulate an approaching two-dimensional object and exhibit firing rate modulation correlated with changes in object trajectory. It is not known how this pathway responds to visual expansion of a three-dimensional object or an approaching object that changes velocity, both of which represent natural stimuli. We compared DCMD responses with images that emulate the approach of a sphere with those elicited by a two-dimensional disc. A sphere evoked later peak firing and decreased sensitivity to the ratio of the half size of the object to the approach velocity, resulting in an increased threshold subtense angle required to generate peak firing. We also presented locusts with an approaching sphere that decreased or increased in velocity. A velocity decrease resulted in transition-associated peak firing followed by a firing rate increase that resembled the response to a constant, slower velocity. A velocity increase resulted in an earlier increase in the firing rate that was more pronounced with an earlier transition. These results further demonstrate that this pathway can provide motor circuits for behaviour with salient information about complex stimulus dynamics.

KEY WORDS: Collision detection, DCMD, Locust, 3D shape, Approach velocity

INTRODUCTION

Animals living in complex, spatiotemporally dynamic visual environments require robust collision-detection systems to successfully orient amongst stationary objects and conspecifics as well as to avoid threats, such as an approaching predator. Behavioural and neural mechanisms underlying collision detection and avoidance have been well studied in taxonomically diverse animals, including humans (Gray and Regan, 1998; Poljac et al., 2006; Vallis and McFadyen, 2005) and other primates (Cléry et al., 2017), cats (Liu et al., 2011b), mice (De Franceschi et al., 2016; Shang et al., 2015; Zhao et al., 2014), birds (Cao et al., 2004; Sun and Frost, 1998), frogs (Yamamoto et al., 2003), fish (Dunn et al., 2016; Preuss et al., 2006; Temizer et al., 2015), crustaceans (Carbone et al., 2018; Oliva et al., 2007; Scarano et al., 2018), insects (Gabbiani et al., 1999; von Reyn et al., 2017; Robertson and Johnson, 1993; Santer et al., 2012; Sato and Yamawaki, 2014;


Thyselius et al., 2018; Wang et al., 2018) and sea urchins (Kirwan et al., 2018). Findings suggest that common neural coding strategies exist across these groups and demonstrate the utility of a tractable system to address questions of how complex visual stimuli are detected and how the information is used to drive downstream motor elements to produce adaptive behavioural responses.

Locusts flying in high-density swarms (Uvarov, 1977) must contend with complex visual cues to avoid collision with conspecifics or capture by predators. Flight avoidance behaviour (Robertson and Johnson, 1993) is controlled by suites of steering muscles that produce either coordinated wing asymmetries to move the locust away from a threat (McMillan et al., 2013) or a glide as a last-ditch attempt to avoid a rapidly approaching object (Santer et al., 2005). Collision detection involves a highly tractable system of retinotopic inputs from the eye onto the lobula giant movement detector (LGMD) (O'Shea and Williams, 1974) and its postsynaptic partner, the descending contralateral movement detector (DCMD), which conveys information in a one-to-one spike train from the LGMD (O'Shea and Williams, 1974) to flight circuits in the thorax (Simmons, 1980). Whereas the LGMD/DCMD pathway is preferentially tuned to the visual image of an object approaching along a direct collision course (Hatsopoulos et al., 1995; Rind and Simmons, 1992), such as a predator (Santer et al., 2012), DCMD firing rate dynamics also track changes in object trajectory (McMillan and Gray, 2012), and are affected by the presence of background visual flow (Silva et al., 2015). LGMD responses to looming are produced through combined excitatory and inhibitory inputs (Rind and Bramwell, 1996; Rind et al., 2016) that shape the response profile to produce a peak firing rate at a fixed delay after the object has reached a threshold angle (Jones and Gabbiani, 2012), and the time of peak firing is highly correlated with the ratio of the half size of the object (l) to its absolute approach velocity ($|v|$) (Gabbiani et al., 1999). In this model, feedforward inhibition encodes angular size of expansion whereas feedforward excitation encodes angular velocity (Wang et al., 2018).

Although known elements of the LGMD/DCMD pathway have provided unparalleled information on mechanisms underlying collision detection, the stimuli used consisted primarily of computer-generated images with edge expansion properties that emulate an approach of a two-dimensional (2D) object. These images expand with an angular size (θ) as a function of the inverse tangent of the ratio of the diameter over the distance from the eye. In the natural world, animals are presented with three-dimensional (3D) objects that, on a collision course, expand with the inverse sine of the diameter over the distance and thus increase in angular size relatively later during an approach. The resulting difference in expansion between 2D and 3D objects would likely influence DCMD responses owing to modulation of elements of the model described above. Therefore, we tested the hypothesis that, compared with a disc, different expansion properties of a looming sphere will evoke a greater and later peak DCMD firing rate that will be narrower, have shorter rise and decay phases, and generate fewer spikes.

Department of Biology, University of Saskatchewan, Saskatoon, Saskatchewan, Canada S7N 5E2.

*Author for correspondence (jack.gray@usask.ca)

 J.R.G., 0000-0001-9079-7962

Received 25 August 2018; Accepted 12 October 2018

List of symbols and abbreviations

2D	two-dimensional
3D	three-dimensional
C	constant velocity
C_M	Michelson contrast ratio
d	decay phase
D	decrease in velocity
DCMD	descending contralateral movement detector
I	increase in velocity
/	half size of the object
LGMD	lobula giant movement detector
p	peak DCMD firing rate
PSTH	peristimulus time histogram
PWHM	PSTH width at half the maximum firing rate
r	rise phase
t_{15}	time of last spike before firing rate decreased to 15% of peak value
t_{95}	time when PSTH last increased above 95% confidence interval with positive slope
TOC	time of collision
TOT	time of velocity transition
$ v $	absolute approach velocity
δ	response delay
θ	subtense angle

In addition to 3D shape, many objects in the natural world do not approach along a constant velocity. During an attack, locust predators may change their approach velocity (Santer et al., 2012), which could be a strategy to increase the probability of capture. In *Drosophila*, bimodal escape behaviours evoked by different object approach velocities are controlled through timing of giant fibre interneuron spikes relative to spikes in parallel circuits that evoke one of two escape strategies (von Reyn et al., 2014, 2017), suggesting that behaviour decisions can be made at the level of descending sensory pathways. Given that locust DCMD firing rate modulation correlates with changing stimulus dynamics during an approach (McMillan and Gray, 2012), it is reasonable to assume that changes in approach velocity will also influence spike trains that carry information to motor centres that produce avoidance behaviours. Therefore, we also tested the hypothesis that a velocity change will modulate the DCMD firing rate, which will subsequently track the new velocity.

Using extracellular recordings, we found that, similar to a looming disc, the DCMD responded to a looming sphere with an increasing firing rate that reached a peak before collision. Whereas the peak amplitude was not affected by shape, a sphere evoked a significantly later peak that was less sensitive to changes in $|v|$, resulting in an increased threshold angle to generate the peak. The delay following the threshold angle to the peak was not affected. We also found that the DCMD responded to a velocity decrease with a decreased firing rate that subsequently increased to match expansion from a new, slower approach velocity. A velocity increase evoked an increased firing rate that matched that of a response to the faster constant velocity, though the effect was influenced by the time of the velocity change. We discuss these findings in the context of visual motion coding and how they expand our understanding of neural control of adaptive avoidance behaviour.

MATERIALS AND METHODS**Animals**

We used adult male *Locusta migratoria* (Linnaeus 1758) reared in a crowded colony maintained at the Department of Biology

at the University of Saskatchewan. Locusts were raised at 25–28°C under a 12 h:12 h light:dark cycle with experiments performed during the locusts' light cycle to avoid any modifications in neural responses that could arise from night cycle activity. Experiments were carried out at room temperature (approximately 25°C).

Preparation

The locust's legs were removed and the wings were restrained preceding the attachment of a rigid tether to the ventral thorax using low melting point beeswax. A segment of ventral cervical cuticle was removed to expose a portion of the ventral nerve cord anterior to the prothoracic ganglion. Following nerve cord exposure, the locust was moved to the recording stage. We used a single silver wire hook electrode, insulated with a mixture of Vaseline and mineral oil, to record activity from the right ventral nerve cord, contralateral to the left eye. A silver wire ground electrode was inserted into the abdomen. Locusts were then positioned dorsal side up, with the rostral end 12 cm away from and facing the apex of a rear projection dome screen (diameter=72 cm). We designated the coordinate system such that 0 deg was directly in front of the locust, +90 deg was at the centre of the right eye and –90 deg was at the centre of the left eye. Locusts were left unstimulated against a solid white background before visual stimulation. To prevent neuronal habituation, we maintained an inter-stimulus interval of 3 min.

Stimulus generation

We created visual stimuli using Pyglet, a library in the Python programming language commonly used to create video graphics and animation, and projected images onto the dome screen using an InFocus DepthQ projector (with colour wheel removed) and a GeForce GTX 660 video card. Images were rendered at 100 frames s^{-1} . For four of 14 locusts in experiments testing effects of object shape and all trials testing velocity changes, images were projected at 60 frames s^{-1} . Although this is below the light-adapted flicker fusion frequency of the locust eye (Miall, 1978), the 50 ms Gaussian filter we used to generate peristimulus time histograms (PSTHs; see below) filtered out firing fluctuations that may have phase-locked with the stimulus. For 10 of 14 locusts in experiments testing effects of object shape, the images were projected at 85 frames s^{-1} and the resulting DCMD responses were indistinguishable from those presented at a refresh rate of 60 frames s^{-1} . Additionally, locust DCMD responses to looming stimuli are similar at image refresh rates of 200 and 67 Hz (Gabbiani et al., 1999). Therefore, we are confident that responses accurately reflect effects of the stimulus manipulation we used. The Python code created accounted for dome curvature to render simulated objects with the correct perspective. We projected images of a 14 cm diameter black disc or sphere (Fig. 1A, luminance=1 cd m^{-2}) against a white background (luminance=172 cd m^{-2}) resulting in a Michelson contrast ratio (C_M) of 0.99. Approaches started 500 cm away from the locust's left eye at –45 deg within the azimuthal plane, stopped at the time of projected collision (TOC) and remained on the screen for 1 s. Within the Pyglet code, we rendered each stimulus frame such that the calculated subtense angle (θ) of the disc was:

$$\theta = 2 \tan^{-1} \left(\frac{d}{2D} \right), \quad (1)$$

where d is the diameter (14 cm) and D is the distance from the centre of the disc to the locust eye. We calculated the subtense angle of the

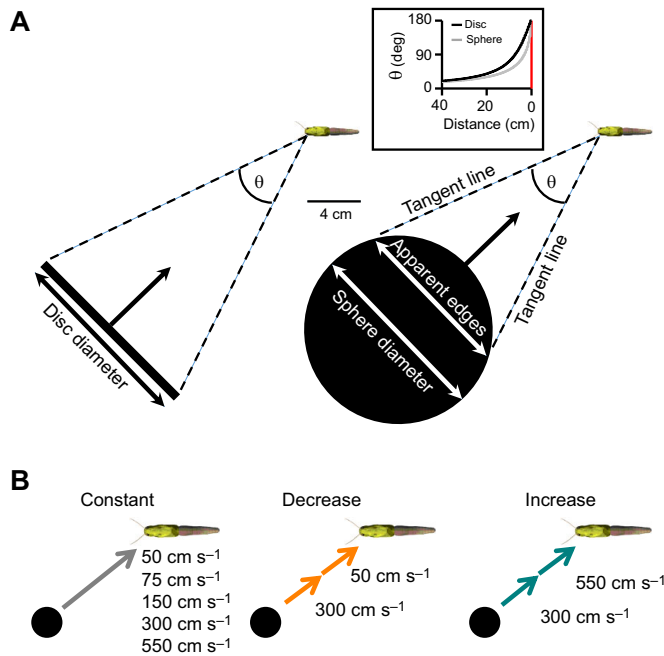


Fig. 1. Visual stimuli. (A) Scaled image of a 14 cm diameter black disc (edge-on view-left) or sphere (right) approaching at -45° within the locust's left visual field. The arrow indicates the direction of motion toward the locust's left eye. The subtense angle (θ) was calculated using the disc diameter (disc) or apparent edges (sphere; see Materials and Methods). The inset shows θ at a distance from 40 cm away to point of collision for a disc (black line) and sphere (grey line). (B) Approach velocities that were constant (50, 75, 150, 300 or 550 cm s^{-1} , grey arrow), decreased (300 to 50 cm s^{-1} , orange arrows) or increased (300 to 550 cm s^{-1} , cyan arrows). The times of instantaneous velocity changes are described in Materials and Methods. Image of sphere not to scale.

sphere based on the apparent edges from the tangent points relative to the locust eye using the equation:

$$\theta = 2 \sin^{-1} \left(\frac{d_{\text{act}}}{2D} \right), \quad (2)$$

where d_{act} is the actual diameter of the sphere (14 cm) and D is the distance of the centre of the sphere to the locust eye. Because the locust was positioned 12 cm from the apex of the dome (radius=31 cm), we were able to create a final subtense angle of 180 deg, thus accurately producing a perceived TOC.

Neural recordings

We recorded neural activity from the right ventral nerve cord (Fig. 2) for each stimulus and amplified the signal with a differential AC amplifier (A-M Systems, model no. 1700, 100 Hz high pass and 5 kHz low pass filters, gain=100 \times). For the first dataset, testing the effects of object shape ($n=14$ locusts), we sampled recordings at 20 kHz, digitized with a Data Translation DT9818 data acquisition board (Techmatron Instruments, Inc., Laval, Canada) interfaced with DataView version 11 acquisition and analysis software (W. J. Heitler, University of St Andrews, UK), and used threshold detection in DataView to discriminate DCMD spikes, which are the largest within the ventral nerve cord. Given the duration of data collection for each locust in this dataset (150 min), it was necessary to use a different group of locusts ($n=20$) to examine DCMD responses to a change in the velocity of a sphere. For this second dataset, we sampled recordings at 25 kHz, digitized with an RP2.1 enhanced real-time processor (Tucker-Davis Technologies, Alachua, FL, USA), and

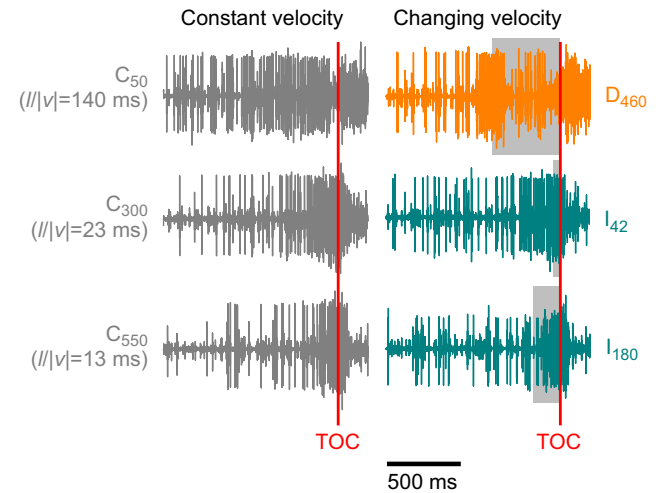


Fig. 2. Raw neural recordings. Data from one locust presented with each of six stimuli. Dark grey traces are responses to constant velocity approaches at 50, 300 or 550 cm s^{-1} (C_{50} , C_{300} or C_{550} , respectively). The orange trace is a response to an approach that slowed from 300 to 50 cm s^{-1} (stimulus D_{460}). The cyan traces are responses to approaches that increased in velocity from 300 to 550 cm s^{-1} , either 42 ms (middle trace, I_{42}) or 180 ms (bottom trace, I_{180}) before the time of collision (TOC; red vertical line). Light grey shaded areas in the right column of traces indicate time windows when the sphere travelled at the slower or faster approach velocities.

used threshold detection in Offline Sorter (Plexon Inc., Dallas, TX, USA) to discriminate DCMD spikes. For both datasets, we created PSTHs from DCMD spike times using Neuroexplorer spike train analysis software (NEX Technologies, Plexon Inc.) using a 1 ms bin width and a 50 ms Gaussian smoothing filter (Guest and Gray, 2006).

Visual stimuli and analysis

Object shape

To examine the effects of object shape on DCMD firing properties and the relationship between the time of peak firing and $1/|v|$, we presented each locust ($n=14$) with a disc or sphere approaching from -45° azimuth against a solid white background at one of five constant velocities (50, 75, 150, 300 and 550 cm s^{-1}), corresponding to $1/|v|$ values of 140, 93, 47, 23 and 13 ms, respectively (Fig. 1B, left panel). We presented three replicates of each stimulus and all stimuli in a random order unique to each locust. Therefore, each locust was presented with 30 approaches, separated by 3 min intervals to avoid DCMD habituation (Gray, 2005). To test for putative effects of object shape on DCMD responses, we compared the peak (p) DCMD firing rate and peak time relative to collision, the width of the PSTH at half the maximum firing rate (PWHM), and the number spikes from the start of object motion to TOC (Fig. 3A). The rise phase (r) was calculated as the time from when the histogram last crossed the 95% confidence interval (grey dashed horizontal line) with a positive slope (t_{95}) to the peak firing rate. The decay phase (d) was calculated as the time from the peak firing rate to when the last spike occurred (arrowhead above raster) prior to the firing rate decreasing to 15% of the peak (t_{15}). We also plotted the time of peak firing against $1/|v|$ for each shape to determine whether the relationship to approaches of a sphere was consistent with that reported for 2D objects (Gabbiani et al., 1999).

Velocity change

We presented a sphere from an azimuthal angle of -45° at either constant or changing velocities (Fig. 1B). The six types of stimuli

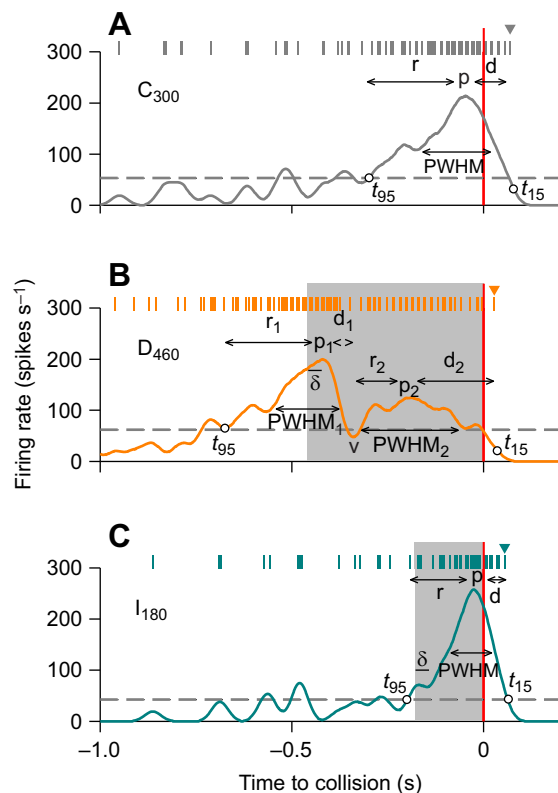


Fig. 3. Descending contralateral movement detector (DCMD) response parameters. Data are from single approaches to the same locust presented with three different velocity types: (A) constant velocity at 300 cm s⁻¹; (B) velocity decreasing from 300 to 50 cm s⁻¹, 460 ms before collision; and (C) velocity increasing from 300 to 550 cm s⁻¹, 180 ms before collision. Top rasters in each panel indicate DCMD spike times and the graph indicates the PSTH of the single spike train. The light grey shaded areas indicate the time window when the sphere travelled at the slower or faster approach velocities. Response parameters: p, p₁, p₂ – peak firing rate for single, first or second peak, respectively; PWHM, PWHM₁, PWHM₂ – duration of peak width at half maximum for single, first or second peak, respectively; t₉₅ – time when PSTH last increased above 95% confidence interval with positive slope; t₁₅ – time of last spike (arrowhead above raster) before firing rate decreased to 15% of peak value; r, r₁, r₂ – rise phase to single, first or second peak, respectively; d, d₁, d₂ – decay phase following single, first or second peak, respectively; v – valley of firing rate; δ – response delay following velocity change. See Materials and Methods for calculation of parameters.

included constant velocity approaches at 50, 300 or 550 cm s⁻¹ and approaches that decreased in velocity instantaneously from 300 to 50 cm s⁻¹ or increased from 300 to 550 cm s⁻¹. Velocity transitions occurred instantaneously over one stimulus frame. The intermediate velocity of 300 cm s⁻¹ is consistent with the average flight speed of a tethered locust (Baker et al., 1981) and is known to evoke flight steering behaviours in loosely tethered locusts (McMillan et al., 2013). The other approach velocities represented stimuli that differentially affect DCMD responses to looming (Gabbiani et al., 2001; Rind and Simmons, 1992). We initially designed velocity changes to occur when the centre of the sphere would have been 100 ms (30 cm) away from the locust eye had it continued at 300 cm s⁻¹. At this time, the leading edge of the sphere (radius=7 cm) was 77 ms (23 cm) away. The time of velocity transition (TOT) was chosen because we intended to examine putative changes in DCMD firing after the response to the initial velocity had begun. The resulting velocity change resulted in a new TOC, which was adjusted based on the position of the leading edge of

the sphere. A decrease from 300 to 50 cm s⁻¹ or increase from 300 to 550 cm s⁻¹ occurred when the leading edge of the sphere was 460 ms before TOC for the decrease (designated D₄₆₀) or 42 ms before TOC for the increase (designated I₄₂). For I₄₂, we observed that at TOT the DCMD firing rate was close to a peak value had the sphere maintained a velocity of 300 cm s⁻¹, which masked putative effects of a velocity change. Therefore, we modified the increasing velocity stimulus regime to also include an increase that occurred when the leading edge was 99 cm (180 ms) away from TOC (designated I₁₈₀).

Throughout the text, we designated abbreviations for the stimulus based on the type of trajectory (constant=C, decrease=D, increase=I), the approach velocity (subscripted as 50, 300 or 550 for constant velocity) and the time of trajectory change (subscripted as 460, 42 or 180 ms). For example, C₃₀₀ indicates a constant velocity approach at 300 cm s⁻¹ whereas D₄₆₀ indicates a velocity that decreased from 300 to 50 cm s⁻¹, 460 ms before collision. For each locust, we presented an initial and final loom at a constant velocity of 300 cm s⁻¹ to determine electrode stability throughout the recording session. We presented each stimulus three times and randomized the sequence uniquely for each locust.

We characterized DCMD firing properties in response to object motion (Fig. 3) using parameters measured from the PSTH response profiles (Gabbiani et al., 2005; McMillan and Gray, 2012; Yakubowski et al., 2016). For approaches at constant (C₅₀, C₃₀₀, C₅₅₀; Fig. 3A) or increasing velocity (I₄₂, I₁₈₀; Fig. 3C), we measured the peak (p) firing rate and peak time relative to TOC, the PWHM, and the number spikes from the start of object motion to TOC. Analysis of PSTH shape was automated using a custom-written program in MATLAB (The MathWorks, Natick, MA, USA). The rise phase (r) was calculated as the time from t₉₅ to the peak firing rate. We also calculated the rate of the firing rate increase to the peak, as measured by the slope from t₉₅ to the peak. The decay phase (d) was calculated as the time from the peak to t₁₅. A velocity decrease (D₄₆₀; Fig. 3B) or velocity increase (I₁₈₀; Fig. 3C) evoked a distinct firing rate peak or local minimum, respectively, soon after the time of transition (TOT; left edge of grey shaded areas), which we measured as the response delay (δ) to the velocity change. Putative firing rate modulation in response to I₄₂ occurred at a time when the firing rate had increased substantially from expansion of the sphere approaching at 300 cm s⁻¹ and, therefore, we were not able to reliably discern δ for I₄₂. For the first peak (p₁) in response to D₄₆₀, we also measured PWHM₁, and the rise phase, r₁ from t₉₅ to the time of p₁. For the second peak (p₂), we measured the firing rate and time (relative to TOC), PWHM₂ and the decay phase (d₂) from time of p₂ to the last spike before t₁₅. The decay phase following p₁ (d₁) and rise phase preceding p₂ (r₂) were calculated relative to the time of the valley (v), which is the lowest firing rate between p₁ and p₂. For D₄₆₀, we also counted the number of spikes from start of object motion to TOC, start of object motion to p₁, and from v to TOC to determine whether the velocity change affected firing properties of the new velocity (50 cm s⁻¹) compared with C₅₀.

For decreasing velocities, we wanted to determine whether the final approach at 50 cm s⁻¹ was similar to a time-matched approach in response to C₅₀. To quantify this possibility, we measured: (1) the firing rate at the time of the valley for D₄₆₀ and compared this with the firing rate at the corresponding time (relative to TOC) for C₅₀; (2) the slope of line from the time of the valley to the time of the second peak for D₄₆₀ and over the corresponding time for C₅₀; and (3) the number of spikes from the valley to TOC for D₄₆₀ and over the corresponding time for C₅₀. For each animal, we used the mean time of the valley from D₄₆₀ as the reference time point for each of three, or fewer, measurements for C₅₀.

Statistical analysis

We used SigmaPlot 12.5 to analyze DCMD firing parameters in response to different projected stimuli. For some recordings (18 of 420 for experiments testing object shape and 12 of 360 for experiments testing velocity changes), the signal to noise ratio was low enough to preclude accurate discrimination of DCMD spikes. In addition, we modified the time to transition for increasing velocities partway through collecting the dataset. For these two reasons, the sample size for each stimulus was not equal across all locusts. Tables S1 and S2 report the total number of presentations and the total number of locusts for each stimulus type for each respective dataset. Because of unequal sample sizes, we tested normally distributed data with a Student's *t*-test (reported with the *t*-value) or a one-way ANOVA (reported with the *F*-value followed by a Holm–Sidak multiple comparison) and graphed results with a column graph. Values that failed tests of normality or equal variance were tested using a Mann–Whitney rank sum test (reported with the *U*-value) or a Kruskal–Wallis ANOVA on ranks (reported with *H*-value followed by a Dunn's multiple comparison) and plotted with box plots. Significance was assessed at $P < 0.05$.

RESULTS

Effects of object shape

The left panels of Fig. 2 show representative traces of DCMD responses to approaches of a sphere at a constant velocity. For each trace, the number of evoked spikes increased during an approach, increasing later at higher velocities, whereas the total number of spikes decreased with increasing velocity.

During an approach, the expansion properties of the disc (black lines) and sphere (grey lines) differed within the same approach velocity (Fig. 4, bottom panels). For a given point in time before collision, the subtense angle of the sphere was smaller than that of the disc, resulting in a more rapid expansion of the sphere near the end of approach. This effect was more pronounced at lower velocities (higher $l/|v|$) and was due to the relatively smaller angular size for the apparent edges of the sphere compared with the diameter of the disc at the same distance from the eye (Fig. 1A, inset). These different expansion properties were reflected in the mean DCMD responses (Fig. 4, top panels). Although the peak firing rate appeared consistent, the time of the peak was progressively later as velocity decreased. To quantify DCMD responses, we calculated,

for each approach, the parameters identified in Fig. 3A. To prevent pseudoreplication, we calculated, for each locust, the mean parameter from the three replicates for each stimulus. These values were then compared across locusts (see Table S1 for sample sizes). Comparing responses between a disc and sphere at each $l/|v|$ value, we found no significant differences in DCMD peak amplitude, PWHM, the number of spikes, the rise phase or the decay phase (data not shown). However, peak time occurred significantly later in response to a sphere for each value of $l/|v|$ (13 ms, $t_{26} = -2.71$; 23 ms, $U_{14} = 26$; 47 ms, $t_{26} = -6.2$; 93 ms, $t_{26} = -4.49$; 140 ms, $t_{24} = -6.01$).

The difference in peak time suggested that object shape affected the relationship with $l/|v|$ (Gabbiani et al., 1999). We calculated the overall regression line for each object type using the peak time from each approach ($n = 35$ –42) for each value of $l/|v|$ (Fig. 5A). We then calculated a single regression line for each locust using the mean peak time of the three replicates of each stimulus and compared the slopes of the lines ($n = 13$ –14) for approaches of a disc or sphere. We found no difference in either the *y*-intercept (disc = 0.8 ± 20 ms, sphere = 7.0 ± 13 ms) or r^2 (disc = 0.97 ± 0.02 , sphere = 0.94 ± 0.09) values of the regressions (data not shown). The mean slope was significantly lower in response approaches of a sphere ($t_{26} = -5.93$; Fig. 5B). We then calculated angular threshold angles for each locust based on eqn 6 of Gabbiani et al. (1999) and found that the threshold angle was significantly higher for a sphere (Fig. 5C). For a disc, θ_{thresh} (41 ± 8.3 deg) was significantly lower than for a sphere (64.3 ± 10.8 deg). These findings demonstrate that DCMD responses to a disc and sphere were similar except that, for a sphere, the peak time was less sensitive to differences in approach velocity and the threshold angle to generate a peak was significantly higher, though the delay (*y*-intercept) was not significantly different.

Effects of velocity changes

Representative traces from individual recordings of DCMD responses to velocity changes (Fig. 2, right panels) showed changes in spiking activity related to the time and type of change. Spike activity increased prior to a velocity decrease (D_{460}), decreased after the transition, and then increased again before TOC. Spiking activity in response to a velocity increase 42 ms before TOC (I_{42}) increased prior to the velocity change and was indistinguishable from activity in response to a constant velocity at

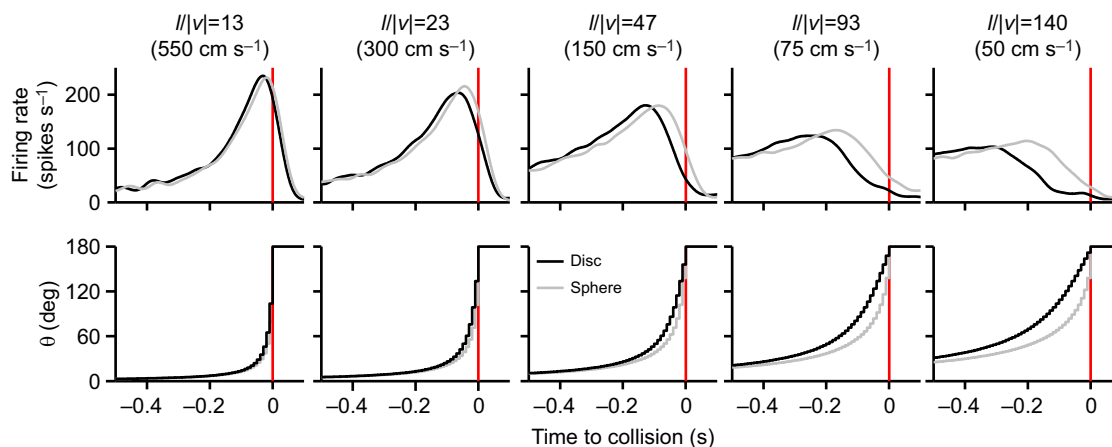


Fig. 4. Effects of object shape on DCMD responses to looming. The top row of plots shows the mean PSTH in response to approaches at five values of $l/|v|$ (and corresponding velocity in cm s^{-1}). $n = 42$ approaches pooled from three velocity replicates for each of 14 locusts. The bottom row of plots shows the change in subtense angle (θ) for each value of $l/|v|$. Data from an approach of a disc or sphere are shown as black or grey lines, respectively. The red vertical lines indicate time of collision.

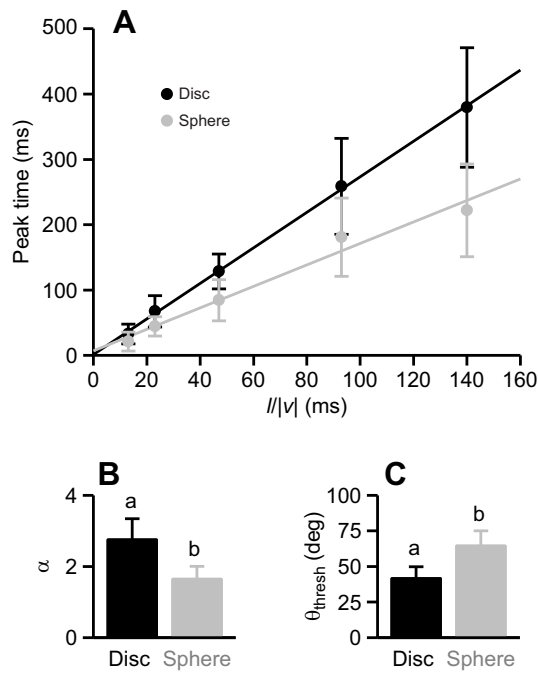


Fig. 5. Object shape affects the relationship between $//|v|$ and peak firing time. (A) Circles and error bars (disc, black; sphere, grey) represent the mean and standard deviation, respectively, from 14 locusts. The peak time for each locust was calculated from the mean of the three replicates of each stimulus. The regression lines were calculated using the peak time from each approach ($N=35\text{--}42$) for each value of $//|v|$. (B) A single regression line for each locust was calculated using the mean of the three replicates of each stimulus. The resulting slopes of the lines ($N=14$) were determined for approaches of a disc or sphere. The mean slope was significantly lower in response to approaches of a sphere. (C) The threshold angle was calculated based on the mean slope for each locust and was significantly higher in response to presentation of a sphere. Bars and error bars represent the mean and positive standard deviation, respectively. Different letters above each bar represent a significant difference (Student's t -test).

300 cm s⁻¹ (C_{300}) whereas an earlier velocity increase (I_{180}) evoked increased spiking activity only after the transition. To examine response profiles across the stimulus types, we plotted the mean PSTHs for the three constant velocities and the velocities that changed (Fig. 6) and time-aligned each with θ . Consistent with data from the previous experiment, the peak time shifted later with higher constant velocity approaches. For all stimuli that included a velocity change, firing rate modulation within the pre-transition epoch resembled that for a time-matched epoch from C_{300} . For D_{460} (Fig. 6, upper right panel), the firing rate peaked soon after the velocity transition, dropped abruptly to a valley, and then increased again, to a relatively lower amplitude peak before TOC. The response profile for I_{42} was indistinguishable from that for C_{300} , whereas for I_{180} , the firing rate increased shortly after the velocity increase to a peak that was similar in amplitude and time compared with C_{550} . For D_{460} and I_{180} , there was a noticeable local deflection in the firing rate shortly after the velocity transition that reflects a response delay (δ ; see Fig. 3).

To demonstrate how a velocity difference or change impacted DCMD activity, we overlaid responses to changes in velocity with those of the component constant velocities, time aligned to the final TOC (Fig. 7). For D_{460} (Fig. 7A), we overlaid the response to C_{300} (shifted to the left by 460 ms) and the response to C_{50} (aligned to TOC). For I_{42} (Fig. 7B) and I_{180} (Fig. 7C), we overlaid the response to C_{300} (shifted to the right by 42 ms or 180 ms, respectively) and

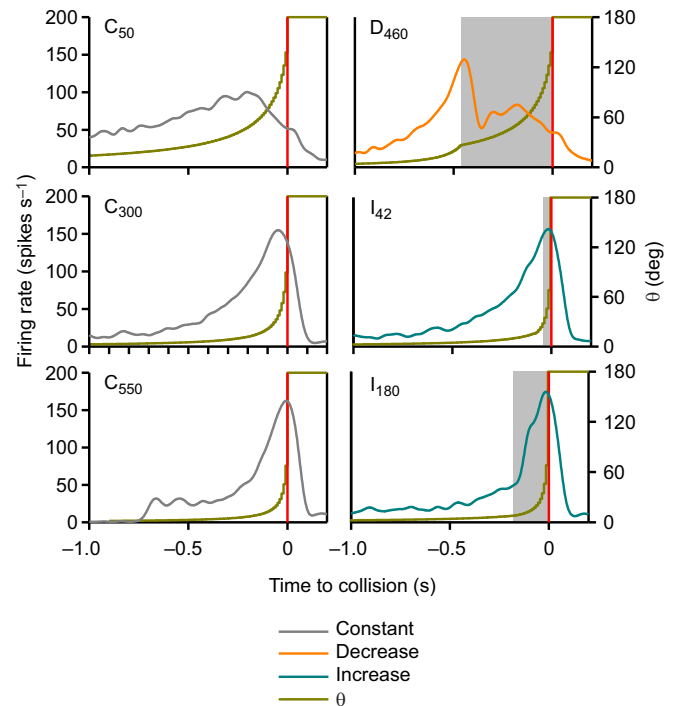


Fig. 6. Mean DCMD responses to approaches at constant or changing velocities. PSTHs used a 1 ms bin width and were smoothed with a 50 ms Gaussian filter. For each panel, the lines depicting the PSTH (grey, orange or cyan) refer to approaches at constant (grey), decreasing (orange) or increasing (cyan) velocities. The gold lines indicate the time-aligned subtense angle (θ). The red vertical line indicates TOC and the light grey shaded areas indicate the time window when the sphere travelled at the slower or faster approach velocities. Velocity designation for each panel is as in Fig. 2. See Table S2 for sample sizes.

the response to C_{550} (aligned to TOC). The overlay for D_{460} and C_{300} showed the decrease in firing rate soon after the transition from 300 to 50 cm s⁻¹, resulting in a peak that occurred earlier than if the object had continued at 300 cm s⁻¹. The overlay for D_{460} and C_{50} showed that the firing rate decreased to a valley for D_{460} , which was lower than the firing rate for C_{50} at the same time. Although the firing rate after the transition to 50 cm s⁻¹ increased again over time, the rise phase was shorter than that for C_{50} , suggesting that the transition reduced the firing rate relative to that in the early stages of a 50 cm s⁻¹ approach. The second peak occurred at the same time, relative to TOC, as for C_{50} . For the overlay of I_{42} , C_{300} and C_{550} (Fig. 7B), the DCMD responses were indistinguishable because the velocity changed close to TOC, at a time when activity was high enough to mask effects of a velocity change. For the overlay of I_{180} , C_{300} and C_{550} (Fig. 7C), the firing rate increased soon after transition to the faster velocity, earlier than if the object had maintained a velocity of 300 cm s⁻¹. The resulting peak in response to the new trajectory was indistinguishable from a peak in response to C_{550} .

To quantify effects of a velocity difference or change on DCMD activity, we compared parameters between different stimuli and found effects depending on whether the velocity decreased or increased (Fig. 8). We found a significant effect of velocity on the peak firing rate ($F_{6,134}=16.9$), peak time ($H_5=83.0$), PWHM ($H_6=46.2$), duration of the rising phase ($H_6=92.7$) and duration of the decay phase ($H_6=74.3$). Significant differences from multiple comparisons of all combinations are indicated in relevant panels of Fig. 8. Specifically, we compared parameters between constant

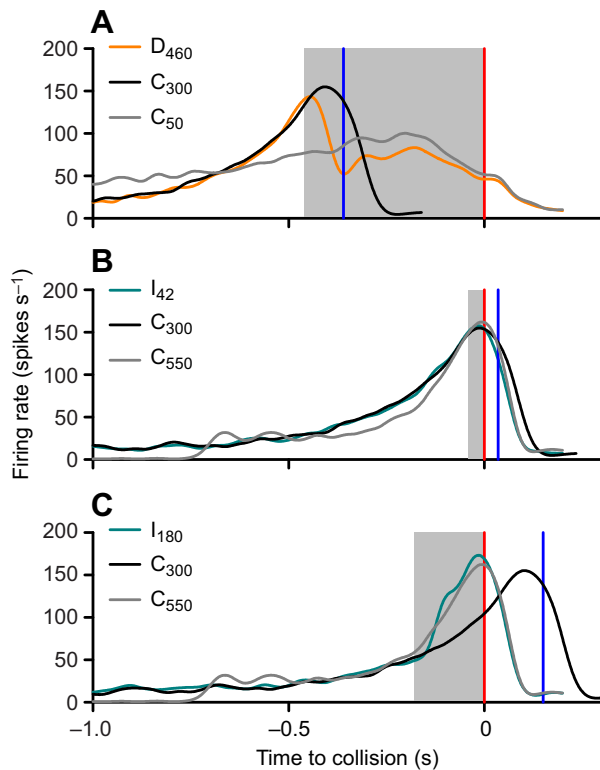


Fig. 7. Overlays of DCMD responses to a velocity decrease or increase with time-adjusted responses to associated constant velocities.

(A) Responses to a velocity decrease. (B) Responses to a velocity increase 42 ms before collision. (C) Responses to a velocity increase 180 ms before collision. The dark grey line represents the response to an approach at a constant velocity of 50 cm s⁻¹ (A) or 550 cm s⁻¹ (B,C). The light grey shaded regions represent the time that the sphere approached at the final velocity and the red vertical line is the associated time of collision for the final velocity. The black line in each plot represents the time-shifted response to an approach at a constant velocity of 300 cm s⁻¹ and the blue vertical line is the corresponding shifted time of collision.

velocities as well as between similar velocities before or after a change: (1) C₅₀, C₃₀₀ and C₅₅₀, (2) C₅₀ and D₄₆₀ p₂, (3) C₃₀₀, D₄₆₀ p₁ and I₄₂, and (4) C₅₅₀ and I₁₈₀. Table 1 summarizes the results of the four types of comparisons and reports whether the difference was a lower or greater value or an earlier or later time. For the first comparison (C₅₀, C₃₀₀ and C₅₅₀), we found that a lower amplitude peak firing rate occurred earlier for C₅₀ compared with C₃₀₀ and C₅₅₀. PWHM for C₅₀ was narrower compared with C₅₅₀ and the rise and decay phases were significantly longer for C₅₀ compared with C₃₀₀ and C₅₅₀. The only difference between C₃₀₀ and C₅₅₀ was a significantly longer PWHM and rise phase for C₃₀₀. For the second comparison (C₅₀ and D₄₆₀ p₂), the only differences were the significantly longer PWHM and rise phase. For the third (C₃₀₀, D₄₆₀ p₁ and I₄₂) and fourth (C₅₅₀ and I₁₈₀) comparisons, the only significant difference was a longer decay phase for C₃₀₀ compared with D₄₆₀ p₁.

A velocity decrease or increase to 550 cm s⁻¹ 180 ms before collision evoked distinguishable response delays associated with the velocity transition (Fig. 3B,C). The delay was longer for an increasing velocity compared with a decreasing velocity (Fig. 9A). We also compared firing parameters at times for C₅₀ comparable to those associated with a firing rate change for D₄₆₀ (see Materials and Methods). We found that compared with C₅₀, a decreasing velocity (D₄₆₀) evoked a lower time-matched firing rate (Fig. 9B), a greater

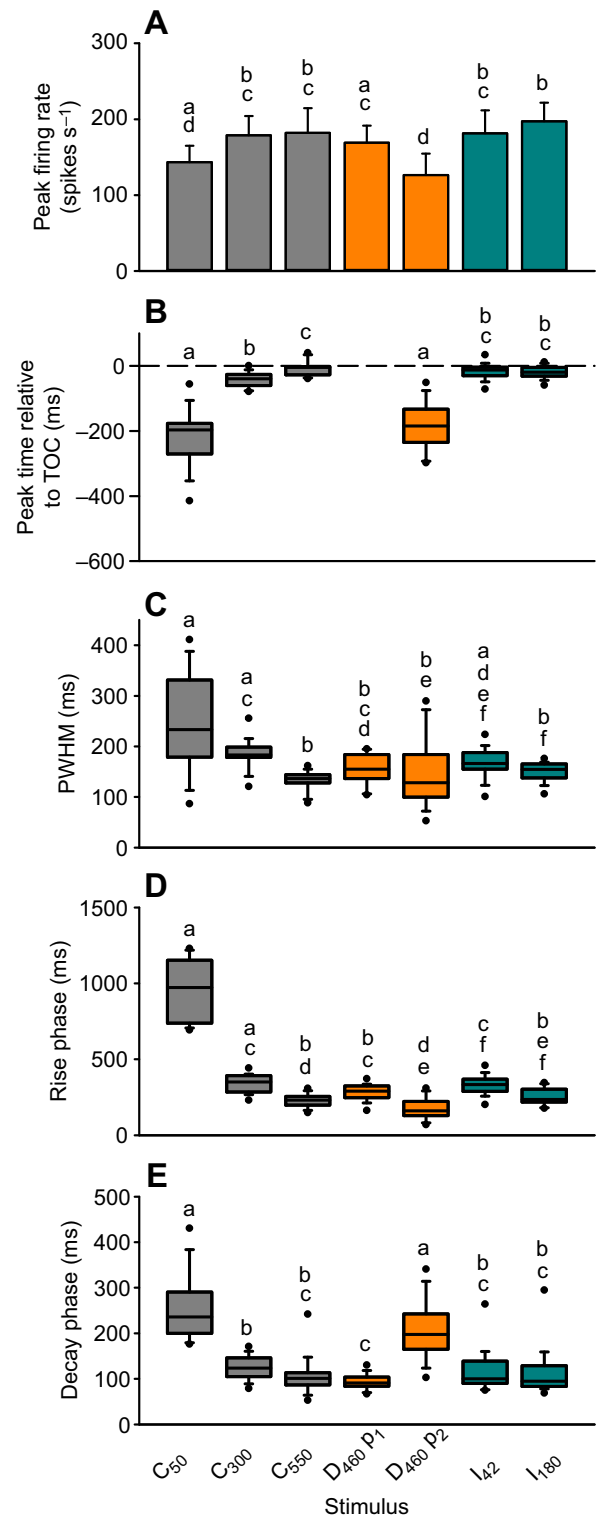


Fig. 8. Summary of DCMD firing parameters. (A) Peak firing rate, (B) time of peak firing, (C) PWHM, (D) rise phase and (E) decay phase (see Materials and Methods for details). Parametric data (A) were tested with a one-way ANOVA followed by a Holm–Sidak multiple comparison between stimulus conditions and presented as means+s.d. Non-parametric data (B–E) were tested with a Kruskal–Wallis one-way ANOVA on ranks followed by a Dunn's multiple comparison between stimulus conditions, and are displayed as box plots with median line, 25th and 75th percentile as box boundaries, 10th and 90th percentiles as error bars, and outliers as small filled circles. Different letters above bars or boxes represent significant differences. See Table S2 for sample sizes.

Table 1. Statistical comparisons of measured DCMD firing parameters in response to velocity changes

Stimulus	Response parameter									
	Peak firing rate		Peak time		PWHM		Rise phase		Decay phase	
	C ₃₀₀	C ₅₅₀	C ₃₀₀	C ₅₅₀	C ₃₀₀	C ₅₅₀	C ₃₀₀	C ₅₅₀	C ₃₀₀	C ₅₅₀
C ₅₀	↓		↓		n.s.	↑	↑	↑	↑	↑
C ₃₀₀		n.s.		n.s.		↑		↑		n.s.
		D ₄₆₀ P ₂		D ₄₆₀ P ₂		D ₄₆₀ P ₂		D ₄₆₀ P ₂		D ₄₆₀ P ₂
C ₅₀		n.s.		n.s.		↑		↑		n.s.
	D ₄₆₀ P ₁	I ₄₂		I ₄₂	D ₄₆₀ P ₁	I ₄₂	D ₄₆₀ P ₁	I ₄₂	D ₄₆₀ P ₁	I ₄₂
C ₃₀₀		n.s.		n.s.	n.s.	n.s.	n.s.	n.s.	↑	n.s.
D ₄₆₀ P ₁		n.s.		n.s.		n.s.		n.s.		n.s.
		I ₁₈₀		I ₁₈₀		I ₁₈₀		I ₁₈₀		I ₁₈₀
C ₅₅₀		n.s.		n.s.		n.s.		n.s.		n.s.

Arrows indicate significant differences: ↓, lower value or earlier time; ↑, greater value or later time. n.s., not significant. See Materials and Methods for stimulus descriptions.

slope of the firing rate increase from the valley to the peak (Fig. 9C), and fewer spikes from the valley to the peak (Fig. 9D). These findings demonstrate that instantaneous changes in velocity of a looming sphere evoked predictable modulation of the DCMD firing rate and that, although components of response phases within compound velocities match responses to component constant velocities, a response delay and resetting occur following transition to a new velocity.

DISCUSSION

Animals orienting in their natural environment must be able to detect dynamic visual motion cues from three-dimensional objects that may represent a threat. Although many experiments have revealed coding properties of motion-sensitive visual circuits, relatively fewer have challenged these circuits with stimulus properties that more closely emulate natural conditions. We tested two hypotheses designed to determine how the well-defined locust visual system responds to different shapes and temporal properties of approaching objects. Our first hypothesis was that, compared with a disc, different expansion properties of a looming sphere would evoke a greater and later DCMD peak firing rate that would be narrower, have shorter rise and decay phases, and generate fewer spikes. We found that although many response parameters, including peak amplitude, were not affected by object shape, the sphere evoked later peak firing, which was less sensitive to changes in $I/|v|$. This lower sensitivity resulted in a significantly higher threshold subtense angle, which is associated with timing of avoidance behaviours (Fotowat et al., 2011). Our second hypothesis was that a velocity change would modulate the DCMD firing rate, which would subsequently track the new velocity. We found that a decrease from 300 to 50 cm s⁻¹ evoked an early peak firing rate following a response delay and that the rate then decreased to a valley, followed by an increase that peaked with dynamics similar to those of a response to a constant velocity of 50 cm s⁻¹. A velocity increase evoked an earlier rise phase following a consistent delay, and the time of the earlier peak depended on the time of the velocity change. To our knowledge, we present the first experimental evidence that responses of a well-described visual motion-detection circuit in the locust are affected by the three-dimensional shape of a looming object. Although changes in constant velocity of single edges have been investigated (Simmons and Rind, 1992), we show that the circuit is also sensitive to changes in edge acceleration resulting from a looming object velocity change during an approach. These findings demonstrate that object shape and approach dynamics are important components when testing responses of motion-sensitive visual circuits.

Comparing response profiles for the same constant velocity approaches of a sphere between the two datasets, the peak firing rate

was higher for approaches at 300 and 550 cm s⁻¹ in the experiments testing the effects of object shape. Given that data come from two distinct groups of locusts, it is possible that the difference is due to variability within the samples. Therefore, we normalized the responses to the maximum firing rates for each respective response to a constant velocity approach at 300 cm s⁻¹. There were no differences in the normalized responses to approaches at 50 or 550 cm s⁻¹, suggesting that the data reported here accurately reflect effects that are due to our manipulation of object expansion properties.

DCMD responses to a disc and sphere

The range of $I/|v|$ values used here (13, 23, 47, 93 and 140) was similar to those used previously (Dewell and Gabbiani, 2018; Dick and Gray, 2014; Gabbiani et al., 2002; Wang et al., 2018), with the lowest value representative of stimuli produced by approaching predators (Santer et al., 2012). For our stimuli that emulated an approaching disc, peak DCMD firing occurred 0.8 ms after the disc reached θ_{thresh} of 41 deg, which is comparable to previous findings (Dick and Gray, 2014; Gabbiani et al., 2001) and relates to timing of behavioural responses to looming (Fotowat et al., 2011). Although expansion of an approaching sphere did not affect the delay for peak DCMD firing, θ_{thresh} was significantly higher at 64 deg. The difference results from the disc expanding as a function of the tangent of the diameter (Eqn 1) whereas the sphere expands as a function of the sine of the apparent edge (Eqn 2). Subsequently, the visual subtense angle increases later during the approach of a sphere, which is more pronounced at lower velocities (Fig. 4). Given that the LGMD/DCMD firing rate during a loom is controlled by coordination of excitatory and inhibitory presynaptic circuits (Rind et al., 2016; Wang et al., 2018; Zhu et al., 2018), expansion of a sphere would activate the pathway along a different time course. Specifically, feedforward inhibition that defines the time of peak firing inhibition when θ passes ~23 deg (Gabbiani et al., 2005) would occur later in response to a sphere. Peak amplitude, however, was not affected by object shape (Fig. 4), suggesting that presynaptic excitation was similar for both shapes and that expansion of a sphere is not simply reflective of a disc with a different $I/|v|$ value. Altered sensitivity of the LGMD/DCMD pathway to $I/|v|$ for a sphere suggests that, for a given approach velocity, either coordinated behavioural responses (McMillan et al., 2013) would be evoked later for 3D objects than for a similarly shaped 2D object, or 'last-ditch' gliding behaviours (Santer et al., 2005) may predominate. For example, when evaluating attack behaviours of wild black kites and emulating the looming stimulus with black discs, Santer et al. (2012) showed that glide behaviour

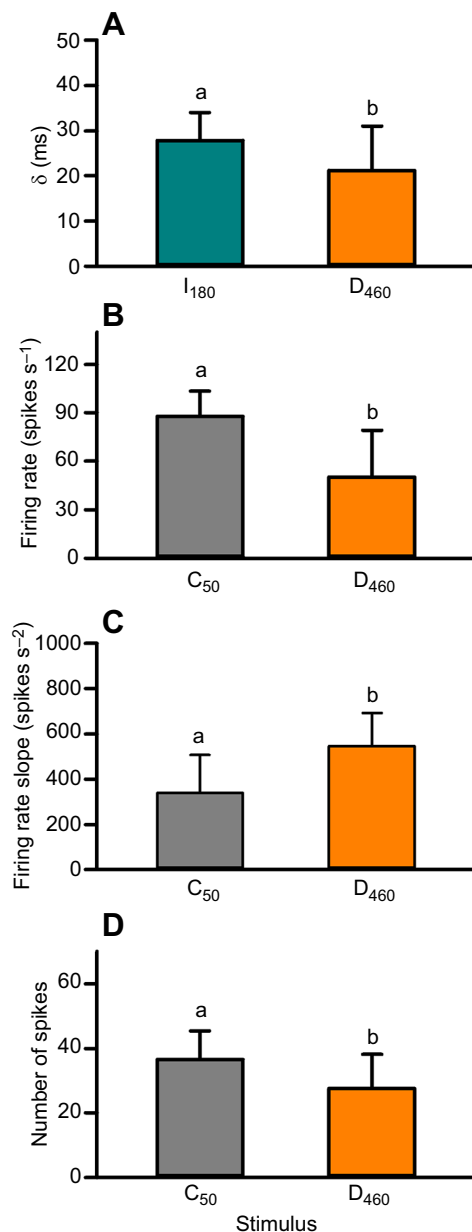


Fig. 9. Response delay and comparison of time matched firing rate properties in response to constant and decreasing velocities.

(A) Response delay (δ) for the valley in I_{180} (cyan) and the first peak in D_{460} (orange). (B) Firing rate at the time of the valley in response to a decreasing velocity (orange) and at the corresponding time (calculated for each locust) in response to a constant velocity at 50 cm s^{-1} (grey). (C) Slope of line from the time of the valley to the time of the second peak for decreasing velocity and over the same time window for constant velocity. (D) Number of spikes from the valley to TOC for decreasing velocity and over the same time window for constant velocity. Data were tested with a Student's *t*-test. See Table S2 for sample sizes. Different letters above bars represent significant differences.

decreased with lower values of $l/|v|$ (faster approaches). Behavioural experiments are needed to test this hypothesis and explore adaptive predator–prey strategies with simulated 3D objects approaching at different content or changing velocities.

DCMD responses to velocity change

DCMD responses to a decreasing approach velocity can be explained by known properties of circuits presynaptic to the

LGMD and are consistent with decreased spiking in response to linear edge expansion resulting from a continually decelerating approaching object (Hatsopoulos et al., 1995; Rind, 1996). The response we observed is similar to a spike rate decrease following rapid onset of background visual flow approximately 260 ms before collision (see fig. 2C of Gabbiani et al., 2002), which activates postsynaptic inhibition of the LGMD. Recent findings show that feedforward inhibition encodes angular size whereas feedforward excitation encodes angular velocity (Wang et al., 2018). Here, we show that at TOT for D_{460} , θ changed from 27 to 27.4 deg, decelerating from an expansion velocity (θ') of 285 to 47 deg s^{-1} (acceleration, $\theta'' = -23,800 \text{ deg s}^{-2}$), which would decrease activation of retinotopic (Peron et al., 2009) and feedforward (Wang et al., 2018) excitatory inputs. At this time, θ surpassed a threshold angle for activating feedforward inhibition (23 deg; Gabbiani et al., 2005), resulting in an imbalance of inhibition over excitation and causing the firing rate to decrease rapidly. Subsequent edge expansion at the new, slower approach velocity would reactivate excitatory circuits while inhibition remained strong, creating a distinct valley in the PSTH. At the new approach velocity, the firing rate increase reached a peak 175 ms before collision ($\theta = 52 \text{ deg}$), which is consistent with responses to a constant velocity approach of 50 cm s^{-1} . The firing rate increased faster after TOT than for the same time window for C_{50} , which could be due to continued, though lower, excitation prior to TOT.

Responses to increased object velocity are likely controlled primarily by feedforward inhibition to the LGMD. For I_{42} , feedforward inhibition would have been activated approximately 10 ms before TOT, which occurred relatively late in the approach. Therefore, any effect of increased excitation from positive θ'' would be minimal in the face of strong inhibition, and the peak firing rate and time would be unaffected. For I_{180} , feedforward inhibition would have been activated 50 ms before TOC (130 ms after TOT). Before TOT, the firing rate would have been driven primarily by relatively weak excitation, whereas after TOT, excitation would have increased substantially with increasing edge velocity, evoking a response profile consistent with a constant velocity approach at 550 cm s^{-1} .

Motion detection and escape behaviour

DCMD responses to changes in object motion reported here add to our understanding of how this pathway is adapted to complex natural stimuli, including changes in object trajectory (Dick and Gray, 2014; McMillan and Gray, 2012; Yakubowski et al., 2016). Our findings also have implications for general mechanisms of motion detection because size threshold encoding strategies are similar across many systems, including visual projection neurons of flies (de Vries and Clandinin, 2012), crabs (Carbone et al., 2018; Oliva and Tomsic, 2014) and the praying mantis (Sato and Yamawaki, 2014), as well as in the optic tectum of zebrafish (Dunn et al., 2016) and pigeons (Wu et al., 2005), and there is a positive linear relationship between the time of peak neural firing and $l/|v|$ (Sun and Frost, 1998). Therefore, it is possible that the responses reported here may be ubiquitous across taxa and provide one of a suite of neural mechanisms for behavioural selection. For example, a delay in spike timing between the left and right Mauthner cells of larval zebrafish determines whether the escape motor pattern will be a C-start or an S-start (Liu and Hale, 2014; Liu et al., 2011a) through subsequent recruitment of downstream motor neurons that override swimming (Song et al., 2015). Within a retinotopic network of looming selective neurons in *Xenopus* tadpoles, modulation of individual tectal cells may predict behavioural choices (Jang et al., 2016). Selection of behavioural

choices involving motion-detection circuits is important in the context of adaptive anti-predator responses given that predator attacks may not always be at constant velocity. In *Drosophila*, one type of visual projection neuron onto giant fibres encodes angular expansion velocity and another type encodes angular size. Feature integration of these two types in giant fibres appropriately biases rapid escapes from predators (von Reyn et al., 2014, 2017). Visual cues may also distinguish the proximity of predators, providing information to adjust escape responses accordingly (De Franceschi et al., 2016; Smolka et al., 2011; Thyselius et al., 2018; Yilmaz and Meister, 2013). In this context, our findings suggest a mechanism to determine whether an object slows down or speeds up during an approach and adjust flight behaviour accordingly. A velocity decrease could allow the LGMD/DCMD pathway time to evoke a coordinated escape flight steering response (Chan and Gabbiani, 2013; McMillan et al., 2013), whereas a velocity increase would evoke a last-ditch glide (Santer et al., 2005). Changes in object velocity could also reflect self-motion through changes in locust flight speed and may evoke landing or avoidance behaviours. To further explore potential effects of the LGMD/DCMD pathway on behavioural choice, experiments are needed to test specific hypotheses on behaviour responses to different object shapes (2D or 3D) and changes in object velocity and trajectory. Manipulating object contrast while varying approach velocity or trajectory would address questions regarding neural coding because DCMD responses are consistent for blurred edges (Jones and Gabbiani, 2010) and sensitive to decreases in object coherence (Dewell and Gabbiani, 2018), each of which likely exist in the natural visual world. Additionally, simultaneous recordings from multiple neurons in the locust (Dick et al., 2017) will allow for a comparative approach to uncovering neural population coding of complex visual environments, which have been investigated in other systems (Dunn et al., 2016; Liu et al., 2011b).

Acknowledgements

We thank C. Manchester, S. Zhang and two anonymous reviewers for providing valuable comments and reviewing an earlier version of the manuscript.

Competing interests

The authors declare no competing or financial interests.

Author contributions

Conceptualization: T.P.S., E.G.N.O., R.H.P., J.R.G.; Methodology: T.P.S., E.G.N.O., J.R.G.; Software: E.G.N.O., R.H.P.; Validation: J.R.G.; Formal analysis: T.P.S., E.G.N.O., R.H.P., J.R.G.; Investigation: T.P.S., E.G.N.O., J.R.G.; Resources: J.R.G.; Data curation: T.P.S., J.R.G.; Writing - original draft: T.P.S., E.G.N.O., R.H.P., J.R.G.; Writing - review & editing: J.R.G.; Visualization: T.P.S., J.R.G.; Supervision: J.R.G.; Project administration: J.R.G.; Funding acquisition: J.R.G.

Funding

Funding was provided by the Natural Sciences and Engineering Research Council of Canada (award number: RGPIN-2014-05269), the Canada Foundation for Innovation (CFI) and the University of Saskatchewan.

Data availability

The Python code for stimulus generation and MATLAB code for automating parameters from neuronal firing rate profiles have been deposited in the Dryad Digital Repository (Stott et al., 2018): <https://doi.org/10.5061/dryad.b1366vs>

Supplementary information

Supplementary information available online at <http://jeb.biologists.org/lookup/doi/10.1242/jeb.191320.supplemental>

References

Baker, P. S., Gewecke, M. and Cooter, R. J. (1981). The natural flight of the migratory locust, *Locusta migratoria* L. III. Wing-beat frequency, flight speed and attitude. *J. Comp. Physiol. A*, **141**, 233-237.

- Cao, P., Gu, Y. and Wang, S. R. (2004). Visual neurons in the pigeon brain encode the acceleration of stimulus motion. *J. Neurosci.* **24**, 7690-7698.
- Carbone, J., Yabo, A. and Oliva, D. (2018). Characterization and modelling of looming-sensitive neurons in the crab *Neohelice*. *J. Comp. Physiol. A* **204**, 487-503.
- Chan, R. W. and Gabbiani, F. (2013). Collision-avoidance behaviors of minimally restrained flying locusts to looming stimuli. *J. Exp. Biol.* **216**, 641-655.
- Cléry, J., Guipponi, O., Odouard, S., Pinède, S., Wardak, C. and Ben Hamed, S. (2017). The prediction of impact of a looming stimulus onto the body is subserved by multisensory integration mechanisms. *J. Neurosci.* **34**, 10656-10670.
- De Franceschi, G., Vivattanasarn, T., Saleem, A. B. and Solomon, S. G. (2016). Vision guides selection of freeze or flight defense strategies in mice. *Curr. Biol.* **26**, 2150-2154.
- de Vries, S. E. J. and Clandinin, T. R. (2012). Loom-sensitive neurons link computation to action in the *Drosophila* visual system. *Curr. Biol.* **22**, 353-362.
- Dewell, R. B. and Gabbiani, F. (2018). Biophysics of object segmentation in a collision-detecting neuron. *eLife* **7**, e34238.
- Dick, P. C. and Gray, J. R. (2014). Spatiotemporal stimulus properties modulate responses to trajectory changes in a locust looming-sensitive pathway. *J. Neurophysiol.* **111**, 1736-1745.
- Dick, P. C., Michel, N. L. and Gray, J. R. (2017). Complex object motion represented by context-dependent correlated activity of visual interneurons. *Physiol. Rep.* **5**, e13355.
- Dunn, T. W., Gebhardt, C., Naumann, E. A., Riegler, C., Ahrens, M. B., Engert, F. and Del Bene, F. (2016). Neural circuits underlying visually evoked escapes in larval zebrafish. *Neuron* **89**, 613-628.
- Fotowat, H., Harrison, R. R. and Gabbiani, F. (2011). Multiplexing of motor information in the discharge of a collision detecting neuron during escape behaviors. *Neuron* **69**, 147-158.
- Gabbiani, F., Krapp, H. G. and Laurent, G. (1999). Computation of object approach by a wide-field motion-sensitive neuron. *J. Neurosci.* **19**, 1122-1141.
- Gabbiani, F., Mo, C. H. and Laurent, G. (2001). Invariance of angular threshold computation in a wide-field looming-sensitive neuron. *J. Neurosci.* **21**, 314-329.
- Gabbiani, F., Krapp, H. G., Koch, C. and Laurent, G. (2002). Multiplicative computation in a visual neuron sensitive to looming. *Nature* **420**, 320-324.
- Gabbiani, F., Cohen, I. and Laurent, G. (2005). Time-dependent activation of feed-forward inhibition in a looming-sensitive neuron. *J. Neurophysiol.* **94**, 2150-2161.
- Gray, J. R. (2005). Habituated visual neurons in locusts remain sensitive to novel looming objects. *J. Exp. Biol.* **208**, 2515-2532.
- Gray, R. and Regan, D. M. (1998). Accuracy of estimating time to collision using binocular and monocular information. *Vis. Res.* **38**, 499-512.
- Guest, B. B. and Gray, J. R. (2006). Responses of a looming-sensitive neuron to compound and paired object approaches. *J. Neurophysiol.* **95**, 1428-1441.
- Hatsopoulos, N. G., Gabbiani, F. and Laurent, G. (1995). Elementary computation of object approach by a wide-field visual neuron. *Science* **270**, 1000-1003.
- Jang, E. V., Ramirez-Vizcarrondo, C., Aizenman, C. D. and Khakhralin, A. S. (2016). Emergence of selectivity to looming stimuli in a spiking network model of the optic tectum. *Front. Neural Circuits* **10**, 831-814.
- Jones, P. W. and Gabbiani, F. (2010). Synchronized neural input shapes stimulus selectivity in a collision-detecting neuron. *Curr. Biol.* **20**, 2052-2057.
- Jones, P. W. and Gabbiani, F. (2012). Logarithmic compression of sensory signals within the dendritic tree of a collision-sensitive neuron. *J. Neurosci.* **32**, 4923-4934.
- Kirwan, J. D., Bok, M. J., Smolka, J., Foster, J. J., Hernández, J. C. and Nilsson, D.-E. (2018). The sea urchin *Diadema africanum* uses low resolution vision to find shelter and deter enemies. *J. Exp. Biol.* **221**, 176271.
- Liu, Y.-C. and Hale, M. E. (2014). Alternative forms of axial startle behaviors in fishes. *Zoology* **117**, 36-47.
- Liu, Y.-C., Bailey, I. and Hale, M. E. (2011a). Alternative startle motor patterns and behaviors in the larval zebrafish (*Danio rerio*). *J. Comp. Physiol. A* **198**, 11-24.
- Liu, Y.-J., Wang, Q. and Li, B. (2011b). Neuronal responses to looming objects in the superior colliculus of the cat. *Brain Behav. Evol.* **77**, 193-205.
- McMillan, G. A. and Gray, J. R. (2012). A looming-sensitive pathway responds to changes in the trajectory of object motion. *J. Neurophysiol.* **108**, 1052-1068.
- McMillan, G. A., Loessin, V. and Gray, J. R. (2013). Bilateral flight muscle activity predicts wing kinematics and 3-dimensional body orientation of locusts responding to looming objects. *J. Exp. Biol.* **216**, 3369-3380.
- Miall, R. C. (1978). The flicker fusion frequencies of six laboratory insects, and the response of the compound eye to mains fluorescent "ripple". *Physiol. Entomol.* **3**, 99-106.
- Oliva, D. and Tomsic, D. (2014). Computation of object approach by a system of visual motion-sensitive neurons in the crab *Neohelice*. *J. Neurophysiol.* **112**, 1477-1490.
- Oliva, D., Medan, V. and Tomsic, D. (2007). Escape behavior and neuronal responses to looming stimuli in the crab *Chasmagnathus granulatus* (Decapoda: Grapsidae). *J. Exp. Biol.* **210**, 865-880.
- O'Shea, M. and Williams, J. L. D. (1974). The anatomy and output connections of a locust visual interneurone: the lobula giant movement detector (LGMD) neurone. *J. Comp. Physiol.* **91**, 257-266.

- Peron, S. P., Jones, P. W. and Gabbiani, F. (2009). Precise subcellular input retinotopy and its computational consequences in an identified visual interneuron. *Neuron* **63**, 830–842.
- Poljac, E., Neggers, B. and Berg, A. V. (2006). Collision judgment of objects approaching the head. *Exp. Brain Res.* **171**, 35–46.
- Preuss, T., Osei-Bonsu, P. E., Weiss, S. A., Wang, C. and Faber, D. S. (2006). Neural representation of object approach in a decision-making motor circuit. *J. Neurosci.* **26**, 3454–3464.
- Rind, F. C. (1996). Intracellular characterization of neurons in the locust brain signaling impending collision. *J. Neurophysiol.* **75**, 986–995.
- Rind, F. C. and Bramwell, D. I. (1996). Neural network based on the input organization of an identified neuron signaling impending collision. *J. Neurophysiol.* **75**, 967–985.
- Rind, F. C. and Simmons, P. J. (1992). Orthopteran DCMD neuron: a reevaluation of responses to moving objects. I. selective responses to approaching objects. *J. Neurophysiol.* **68**, 1654–1666.
- Rind, F. C., Wernitznig, S., Pöhl, P., Zankel, A., Gütl, D., Sztarker, J. and Leitinger, G. (2016). Two identified looming detectors in the locust: ubiquitous lateral connections among their inputs contribute to selective responses to looming objects. *Sci. Rep.* **6**, 35525.
- Robertson, R. M. and Johnson, A. G. (1993). Collision avoidance of flying locusts: steering torques and behaviour. *J. Exp. Biol.* **183**, 35–60.
- Santer, R. D., Simmons, P. J. and Rind, F. C. (2005). Gliding behaviour elicited by lateral looming stimuli in flying locusts. *J. Comp. Physiol. A.* **191**, 61–73.
- Santer, R. D., Rind, F. C. and Simmons, P. J. (2012). Predator versus prey: Locust looming-detector neuron and behavioural responses to stimuli representing attacking bird predators. *PLoS ONE* **7**, e50146.
- Sato, K. and Yamawaki, Y. (2014). Role of a looming-sensitive neuron in triggering the defense behavior of the praying mantis *Tenodera aridifolia*. *J. Neurophysiol.* **112**, 671–682.
- Scarano, F., Sztarker, J., Medan, V., Berón de Astrada, M. and Tomsic, D. (2018). Binocular neuronal processing of object motion in an arthropod. *J. Neurosci.* **38**, 6933–6948.
- Shang, C., Liu, Z., Chen, Z., Shi, Y., Wang, Q., Liu, S., Li, D. and Cao, P. (2015). A parvalbumin-positive excitatory visual pathway to trigger fear responses in mice. *Science* **348**, 1472–1477.
- Silva, A. C., McMillan, G. A., Santos, C. P. and Gray, J. R. (2015). Background complexity affects the response of a looming-sensitive neuron to object motion. *J. Neurophysiol.* **113**, 218–231.
- Simmons, P. J. (1980). Connexions between a movement-detecting visual interneurone and flight motoneurons of a locust. *J. Exp. Biol.* **86**, 87–97.
- Simmons, P. J. and Rind, F. C. (1992). Orthopteran DCMD neuron: a reevaluation of responses to moving objects. II. Critical cues for detecting approaching objects. *J. Neurophysiol.* **68**, 1667–1682.
- Smolka, J., Zeil, J. and Hemmi, J. M. (2011). Natural visual cues eliciting predator avoidance in fiddler crabs. *Proc. R. Soc. B* **278**, 3584–3592.
- Song, J., Ampatzis, K., Ausborn, J. and El Manira, A. (2015). A hardwired circuit supplemented with endocannabinoids encodes behavioral choice in zebrafish. *Curr. Biol.* **25**, 2610–2620.
- Stott, T. P., Olson, E. G. N., Parkinson, R. H. and Gray, J. R. (2018). Data from: Three-dimensional shape and velocity changes affect responses of a locust visual interneuron to approaching objects. Dryad Digital Repository.
- Sun, H. and Frost, B. J. (1998). Computation of different optical variables of looming objects in pigeon nucleus rotundus neurons. *Nat. Neurosci.* **1**, 296–303.
- Temizer, I., Donovan, J. C., Baier, H. and Semmelhack, J. L. (2015). A visual pathway for looming-evoked escape in larval zebrafish. *Curr. Biol.* **25**, 1823–1834.
- Thygesius, M., Gonzalez-Bellido, P. T., Wardill, T. J. and Nordström, K. (2018). Visual approach computation in feeding hoverflies. *J. Exp. Biol.* **221**, jeb177162-j9.
- Uvarov, B. (1977). *Grasshoppers and Locusts. A Handbook of General Acridology. Volume 2. Behaviour, Ecology, Biogeography, Population Dynamics*. London: Centre for Overseas Pest Research.
- Vallis, L. and McFadyen, B. (2005). Children use different anticipatory control strategies than adults to circumvent an obstacle in the travel path. *Exp. Brain Res.* **167**, 119–127.
- von Reyn, C., Breads, P., Peek, M. Y., Zheng, G. Z., Williamson, W. R., Yee, A. L., Leonardo, A. and Card, G. M. (2014). A spike-timing mechanism for action selection. *Nat. Neurosci.* **17**, 962–970.
- von Reyn, C., Nern, A., Williamson, W. R., Breads, P., Wu, M., Namiki, S. and Card, G. M. (2017). Feature integration drives probabilistic behavior in the *Drosophila* escape response. *Neuron* **94**, 1190–1204.
- Wang, H., Dewell, R. B., Zhu, Y. and Gabbiani, F. (2018). Feedforward inhibition conveys time-varying stimulus information in a collision detection circuit. *Curr. Biol.* **28**, 1509–1521.
- Wu, L.-Q., Niu, Y.-Q., Yang, J. and Wang, S. R. (2005). Tectal neurons signal impending collision of looming objects in the pigeon. *Eur. J. Neurosci.* **22**, 2325–2331.
- Yakubowski, J. M., McMillan, G. A. and Gray, J. R. (2016). Background visual motion affects responses of an insect motion-sensitive neuron to objects deviating from a collision course. *Physiol. Rep.* **4**, e12801.
- Yamamoto, K., Nakata, M. and Nakagawa, H. (2003). Input and output characteristics of collision avoidance behavior in the frog *Rana catesbeiana*. *Brain Behav. Evol.* **62**, 201–211.
- Yilmaz, M. and Meister, M. (2013). Rapid innate defensive responses of mice to looming visual stimuli. *Curr. Biol.* **23**, 2011–2015.
- Zhao, X., Liu, M. and Cang, J. (2014). Visual cortex modulates the magnitude but not the selectivity of looming-evoked responses in the superior colliculus of awake mice. *Neuron* **84**, 202–213.
- Zhu, Y., Dewell, R. B., Wang, H. and Gabbiani, F. (2018). Pre-synaptic muscarinic excitation enhances the discrimination of looming stimuli in a collision-detection neuron. *Cell Reports* **23**, 2365–2378.